Journal Name

ARTICLE TYPE

Synthesis, PtS-type structure, and anomalous mechanics of the Cd(CN)$_2$ precursor Cd(NH$_3$)$_2$[Cd(CN)$_4$]†

Chloe S. Coates,[a] Joshua W. Makepeace,[a] Andrew G. Seel,[a] Mia Baise,[b] Ben Slater,[b] and Andrew L. Goodwin[*a]

We report the nonaqueous synthesis of Cd(CN)$_2$ by oxidation of cadmium metal with Hg(CN)$_2$ in liquid ammonia. The reaction proceeds *via* an intermediate of composition Cd(NH$_3$)$_2$[Cd(CN)$_4$], which converts to Cd(CN)$_2$ on prolonged heating. Powder X-ray diffraction measurements allow us to determine the crystal structure of the previously-unreported Cd(NH$_3$)$_2$[Cd(CN)$_4$], which we find to adopt a twofold interpenetrating PtS topology. We discuss the effect of partial oxidation on the Cd/Hg composition of this intermediate, as well as its implications for the reconstructive nature of the deammination process. Variable-temperature X-ray diffraction measurements allow us to characterise the anisotropic negative thermal expansion (NTE) behaviour of Cd(NH$_3$)$_2$[Cd(CN)$_4$] together with the effect of Cd/Hg substitution; *ab initio* density functional theory (DFT) calculations reveal a similarly anomalous mechanical response in the form of both negative linear compressibility (NLC) and negative Poisson's ratios.

1 Introduction

Cadmium(II) cyanide, Cd(CN)$_2$, is remarkable primarily for its extreme isotropic negative thermal expansion (NTE) behaviour; its volume decreases with increasing temperature [1,2] at a rate that is substantially more extreme than that of well-known NTE systems such as ZrW$_2$O$_8$ and Zn(CN)$_2$. [1,3–5] Despite the clear fundamental and technological importance of NTE [6–11] and the magnitude of the response in Cd(CN)$_2$, surprisingly little is known regarding the NTE mechanism in this system. [12,13] For related materials, such as Zn(CN)$_2$, a combination of neutron and X-ray scattering measurements has been instrumental in establishing the origin of NTE. [1,2,5,14–16] Yet Cd(CN)$_2$ is difficult to study in both respects: the neutron absorption cross-section of natural-abundance Cd is famously prohibitive to neutron scattering studies (indeed Cd lining is used as shielding in neutron facilities [17]), and Cd(CN)$_2$ also undergoes rapid degradation in the synchrotron X-ray beam. While little can be done to ameliorate the effects of X-ray beam damage in this case, access to a sample enriched with an appropriate Cd isotope would in principle enable neutron scattering studies of Cd(CN)$_2$ to be performed. Consequently, we sought to develop a synthetic approach that

would allow us to prepare multi-gram quantities of Cd(CN)$_2$ directly from Cd metal enriched in ^{114}Cd, an isotope that is well suited to neutron scattering measurements.

Conventional methodologies for preparing Cd(CN)$_2$ in aqueous media invariably give polycrystalline products contaminated with Cd(OH)$_2$, [18] which is problematic in the context of subsequent neutron-scattering studies not only as an unwanted secondary phase but because additional care would need to be taken to ensure the high levels of deuteration required to minimise incoherent scattering from hydrogen. Consequently we sought to develop an alternative preparation route that avoided aqueous media altogether. The particular approach that piqued our interest was the liquid ammonia method reported for the synthesis of zinc cyanide from zinc metal and mercury cyanide. [19]

Here we show that this liquid ammonia synthesis can indeed be modified to allow H$_2$O-free preparation of Cd(CN)$_2$ directly from cadmium metal. We find that the immediate product formed is actually the previously-unknown compound Cd(NH$_3$)$_2$[Cd(CN)$_4$], which in turn converts to Cd(CN)$_2$ on prolonged heating. Using powder X-ray diffraction we determine the crystal structure of Cd(NH$_3$)$_2$[Cd(CN)$_4$] and find it to adopt an interpenetrating PtS topology. [20,21] We discuss the effect of partial oxidation on the Cd/Hg composition of the intermediate, as well as its implications for the reconstructive nature of the deammination process. Variable-temperature X-ray diffraction measurements allow us to characterise the anisotropic NTE behaviour of Cd(NH$_3$)$_2$[Cd(CN)$_4$] together with the effect of Cd/Hg substitution; *ab initio* density functional theory (DFT) calculations reveal

[a] Department of Chemistry, University of Oxford, Inorganic Chemistry Laboratory, South Parks Road, Oxford OX1 3QR, U.K. Fax: +44 1865 274690; Tel: +44 1865 272137; E-mail: andrew.goodwin@chem.ox.ac.uk
[b] Department of Chemistry, University College London, 20 Gordon Street, London WC1H 0AJ, U.K.
† Electronic Supplementary Information (ESI) available: [details of any supplementary information available should be included here]. See DOI: 10.1039/b000000x/
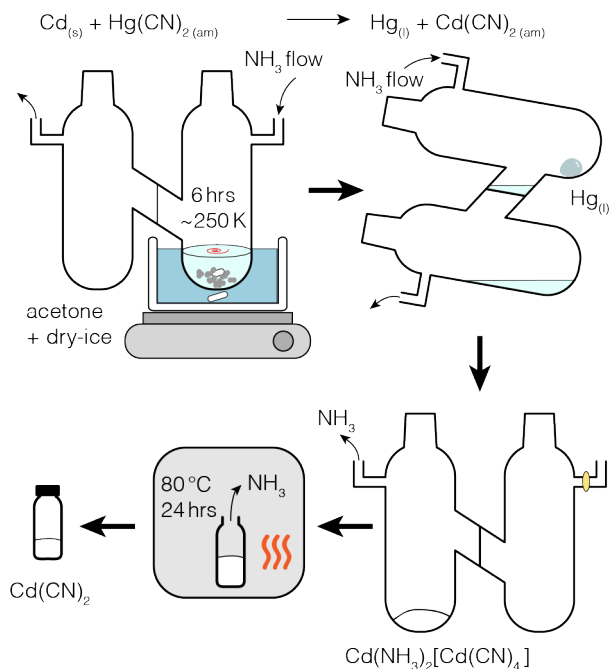
Fig. 1 Reaction scheme for the synthesis of $Cd(CN)_2$ from the redox reaction of excess Cd metal and $Hg(CN)_2$ in liquid ammonia. The reaction was stirred at 240–250 K for six hours and the solution filtered to separate liquid Hg and an ammoniacal solution of $Cd(NH_3)_2[Cd(CN)_4]$. Subsequent evaporation of ammonia yields $Cd(NH_3)_2[Cd(CN)_4]$. On heating, this intermediate compound is converted quantitatively to polycrystalline $Cd(CN)_2$.

an atypical mechanical response in the form of both negative linear compressibility (NLC) and negative Poisson's ratios.[22,23] Our paper concludes with a discussion of the generality of anomalous mechanical responses in PtS-type coordination polymers, and hence the relevance of this structure type as a target for a variety of applications.

2 Methods

2.1 Synthesis

Our synthetic methodology was adapted from that reported in Ref. 19, whereby zinc metal is oxidised by an ammoniacal solution of mercury cyanide to give liquid mercury and zinc cyanide. We condensed anhydrous ammonia gas ($\sim$15 mL) onto 400 mg $Hg(CN)_2$ powder (Aldrich 99 %) and excess Cd metal (400 mg, Fisher 99.9 %) in a custom-made glass N-cell, consisting of two Schlenk tubes separated by a porous frit [Figure 1]. The mixture was stirred for six hours in an acetone/dry-ice bath with the temperature maintained between 240 and 250 K. Following this process a ball of liquid mercury could be seen in the bottom of the flask. The mixture was filtered through the frit under flowing NH_3 gas to give an ammoniacal solution of $Cd(NH_3)_2[Cd(CN)_4]$. The NH_3 was then allowed to evaporate by bringing the system to ambient temperature, yielding a polycrystalline sample of $Cd(NH_3)_2[Cd(CN)_4]$ as a fine white powder. Further heating at 80 °C for 24 hours resulted in complete deammination and quantitative formation of $Cd(CN)_2$ (the same deammination process occurs over a period of 1 month at ambient conditions).

Incomplete reaction of Cd with $Hg(CN)_2$ led to formation of $Cd(NH_3)_2[Cd_xHg_{1-x}(CN)_4]$. The degree of completeness of the oxidation reaction is particularly sensitive to the temperature at which it is carried out and the 240–250 K temperature window represents the optimal balance between ensuring the ammonia remains liquid, on the one hand, and the availability of sufficient thermal energy for the reaction to proceed, on the other hand. Deammination of $Cd(NH_3)_2[Cd_xHg_{1-x}(CN)_4]$ gave a physical mixture of $Hg(CN)_2$ and $Cd(CN)_2$.

2.2 X-ray powder diffraction measurements

X-ray powder diffraction patterns were measured using the I11 beamline at Diamond Light Source (X-ray wavelength $\lambda = 0.82573(1)$ Å, as determined using a Si NIST 640c standard). Samples were loaded into 0.5 mm-diameter borosilicate capillaries and mounted in brass holders to be loaded onto the instrument. Diffraction patterns were collected using a Mythen2 position-sensitive detector, with measurements made at intervals of 10 K between 300 and 100 K. The temperature was controlled using an Oxford Cryostreams attachment. Each measurement consisted of two individual 2-second scans, with the detector offset by $0.25°$ between scans. In order to minimise the effects of sample damage by the synchrotron beam, the capillary was translated horizontally by 2.5 mm for each temperature point such that a fresh sample was irradiated.

2.3 Crystallographic refinements

All fits to powder X-ray diffraction data were carried out in TOPAS Academic.[24] The instrumental contribution to the peak shape function was determined by refining against a Si NIST 640c standard; the final peak shape function took into account this instrumental term and subsequent modification by simple Lorentzian and Gaussian strain terms. Rietveld analysis of the diffraction pattern measured for $Cd(NH_3)_2[Cd_{0.93}Hg_{0.07}(CN)_4]$ at 100 K was carried out with Hg occupancy on the pseudotetrahedral site (Wyckoff position 2b of the $P4_2/mcm$ space group) fixed to the value obtained from refinement of relative molar fractions of $Cd(CN)_2$ and $Hg(CN)_2$ observed in the fully deamminated sample. All atom positions were refined freely (H atoms were omitted) with the isotropic atomic displacement parameters of C and N atoms of the CN^- moiety constrained to be equivalent.

A Pawley refinement was carried out for each dataset collected every 10 K between 300 K to 100 K in space group $P4_2/mcm$. Two capillaries were used in the data collection: capillary 1 from 300-180 K and capillary 2 from 170-100 K. The sample peak shapes were accounted for by convolution with spherical harmonic peak shapes for capillary 1 and with Lorentzian and Gaussian peak shape profiles for capillary 2 in order to obtain the best fit and most accurate lattice parameters. The framework strain induced by gradual deammination can be used to explain the difficulty in modelling the peak shapes observed here, and the slight discrepancy between the two capillaries.

2.4 Quantum mechanical calculations

All density functional theory (DFT) calculations were performed using the Vienna *ab initio* simulation package (VASP).[25–28] Within this quantum mechanical code, a plane-wave basis set was used to model the valence electronic states coupled with a projector-augmented wave (PAW) method which maps the core electrons (treated with pseudopotentials) onto the valence electrons (treated explicitly) to ensure computational efficiency comparable to an all electron method.[29] The Perdew-Burke-Ernzerhof (PBE) exchange-correlation was used because this functional has shown good agreement with experimental data for similar coordination polymers in previous studies.[30] Each calculation employed a plane wave cut-off of 600 eV and a Monkhorst-Pack **k**-point mesh of 4×4×2 to sample the anisotropic cell dimensions. Atom positions and cell parameters were converged simultaneously using the Broyden-Fletcher-Goldfarb-Shanno optimiser; once forces on the atoms were less than 0.01 eV/Angström the system was deemed to have converged.

Our starting point for DFT relaxation was the structure of $Cd(NH_3)_2[Cd(CN)_4]$ obtained from Rietveld refinement of the X-ray diffraction data measured at the lowest temperature accessed experimentally (100 K). This structural model has $P4_2/mcm$ space group symmetry but omits H atoms. The addition of hydrogen atoms lowers the space-group symmetry and therefore all further calculations were performed in $P1$. Following cell relaxation, we checked for the magnitude of symmetry-lowering distortions in the non-hydrogenic component of the structure. The code FINDSYM showed the magnitude of this distortion to be less than 0.01 Å.[31]

The effect of mixed Cd/Hg composition was investigated by considering three systems with the same total composition $CdHg(NH_3)_2(CN)_4$: (i) $Cd(NH_3)_2[Hg(CN)_4]$, (ii) $Hg(NH_3)_2[Cd(CN)_4]$, and (iii) $Cd_{0.5}Hg_{0.5}(NH_3)_2[Cd_{0.5}Hg_{0.5}(CN)_4]$. The plane-wave cut-off, **k**-point mesh and PBE functional used were identical to those given above.

The elastic tensor of $Cd(NH_3)_2[Cd(CN)_4]$ was derived as follows: six finite distortions of the geometry-optimised structure were introduced, and the elastic constants determined from the strain-stress relationship.[32] The elastic tensor was calculated both in the limits of both rigid ions relaxed ion positions. Even without the use of symmetry constraints the resulting elastic properties were found to be almost identical in the **a** and **b** axes, with severe anisotropy relative to the **c** axis—which is as expected for the experimentally-observed tetragonal symmetry. This observation suggests that NH_3 orientations (disordered in our experimental $P4_2/mcm$ structural model) do not affect the mechanical properties of $Cd(NH_3)_2[Cd(CN)_4]$ to any significant extent.

3 Results and discussion

3.1 Synthesis and characterisation of $Cd(NH_3)_2[Cd(CN)_4]$

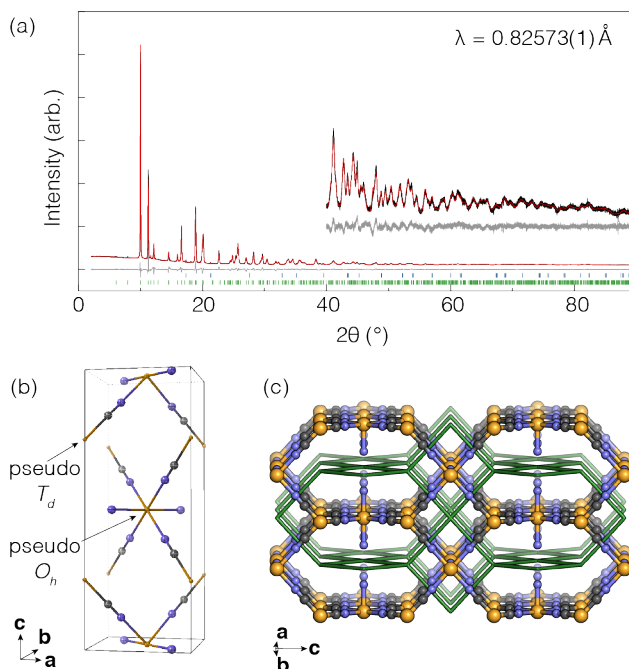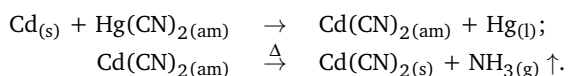Our initial synthetic goal was the oxidation of Cd metal by $Hg(CN)_2$ in liquid ammonia to afford $Cd(CN)_2$ and Hg:

$$Cd_{(s)} + Hg(CN)_{2(am)} \rightarrow Cd(CN)_{2(am)} + Hg_{(l)};$$
$$Cd(CN)_{2(am)} \xrightarrow{\Delta} Cd(CN)_{2(s)} + NH_{3(g)} \uparrow.$$

Fig. 2 (a) Powder X-ray diffraction pattern for $Cd(NH_3)_2[Cd(CN)_4]$ measured at 100 K (black line) and Rietveld fit (red line), with difference (data − fit) shown in grey. The inset shows a 20× magnification of the high-angle data and fit. Green tick marks represent calculated peak positions for $Cd(NH_3)_2[Cd(CN)_4]$ and blue tick marks represent a small impurity of solid α-Hg. (b) Representation of the crystallographic model for $Cd(NH_3)_2[Cd(CN)_4]$ (space group $P4_2/mcm$): Cd centres shown as orange spheres, C in grey and N in blue. Thermal ellipsoids are represented at 50% probability and hydrogen atoms are not shown (nor included in the Rietveld refinement). (c) Topological representation of the framework, following the same colour scheme as in (b), with the second PtS framework shown in green (NH_3 omitted) to highlight the twofold interpenetration.

Following the general procedure of Ref. 19, and the synthesis as described above, we obtained a white polycrystalline product according to this approach. However, the resulting X-ray diffraction pattern of this product [Fig. 2(a)] did not match that expected for $Cd(CN)_2$ (space group $Pn\bar{3}m$, $a_c \simeq 6.3$ Å).[18,33] Instead, by exploring cells with geometries and symmetries related to that of $Cd(CN)_2$, we were able to index the diffraction pattern using a single phase with tetragonal symmetry and

$$a \sim \frac{c}{2\sqrt{2}} \sim \frac{\sqrt{3}}{2}a_c.$$

Pawley refinement gave the lattice parameters $a = 5.93602(8)$ Å and $c = 15.5477(3)$ Å, and suggested systematic absences consistent with the space group $P4_2/mcm$.

The dimensions of this unit cell and the corresponding space group symmetry are reminiscent of those reported previously for $ZnPt(CN)_4$.[34] In this structure type, tetrahedral Zn and square-planar Pt nodes alternate throughout a pair of mutually interpenetrating PtS nets, with each Zn/Pt pair connected by a Zn–NC–Pt linkage. We used the $ZnPt(CN)_4$ structural model of Ref.

Table 1 Structural parameters for $Cd(NH_3)_2[Cd(CN)_4]$ as determined by Rietveld analysis (R_{wp} = 4.328 %) of X-ray powder diffraction data collected at 100 K. Space group: $P4_2/mcm$. Lattice parameters: a = 5.93602(8) Å, c = 15.5477(3) Å. Note that the NH_3 H atoms are assumed to be disordered and are omitted from the refinement

Atom	x	y	z	B_{iso} (Å^2)
Cd1	0.5	0.5	0	0.97(8)
Cd2	0	0	0.25	0.51(6)
C	0.8180(10)	0.1820	0.8418(4)	2.04(10)
N1	0.7129(9)	0.2871	0.8928(3)	2.04
N2	0.2116(8)	0.2116	0	2.2(2)

Fig. 3 X-ray powder diffraction data collected (a) before and (b) after heating a sample of $Cd(NH_3)_2[Cd(CN)_4]$ at 80°C for 24 h. Data (background subtracted) are shown in black, with Rietveld fit shown in red and the difference in grey. Red tick marks represent the calculated peak positions of $Cd(CN)_2$ and blue tick marks those of $Hg(CN)_2$. Refinement of the weight percentage of the $Cd(CN)_2$ product reveals the amount of Hg in the ammoniated intermediate $Cd(NH_3)_2[Cd_xHg_{1-x}(CN)_4]$.

34 as a starting point for Rietveld analysis of our X-ray diffraction pattern, replacing each of Zn and Pt atoms by Cd. We obtained a good fit-to-data, which could be improved further by including additional N atoms (representing rotationally-disordered NH_3 molecules) at a distance of approximately 2 Å from the 'square planar' Cd site. This addition felt chemically sensible since square-planar coordination by cyanide is common for Pt^{II} (d^8) but not for Cd^{II} (d^{10}); our model gives instead an effective octahedral coordination at this originally square-planar site, and octahedral geometry is one of the two typical coordination geometries for Cd^{II} in cyanide frameworks (the other is tetrahedral).[35,36]

The final Rietveld fit is shown in Fig. 2(a) and the corresponding atom coordinates and atomic displacement parameters are listed in Table 1. Hydrogen atoms were not included in this model; our X-ray data are not sufficiently sensitive to their positions, and one might expect the rotational state of NH_3 molecules to be disordered at room temperature anyway. A representation of the crystallographic unit cell of our structure is shown in Fig. 2(b). Note that there are two crystallographically distinct Cd sites in this structure. One has pseudotetrahedral coordination by four cyanide ions, and the other has pseudooctahedral coordination by four cyanide ions and two ammonia molecules. The two sites are present in equal concentrations such that the composition is given by the formula $Cd(NH_3)_2[Cd(CN)_4]$. We will come to show that this particular sample actually contains a very small fraction (3.7 wt%) of Hg substitution on the pseudotetrahedral site such that the correct formula is actually $Cd(NH_3)_2[Cd_{0.93}Hg_{0.07}(CN)_4]$; we will continue to use the formulation $Cd(NH_3)_2[Cd(CN)_4]$ hereafter. Drawing on analogies to the $Cd(CN)_2$ clathrates, our structural model contains cyanide ions with ordered orientations: the pseudotetrahedrally-coordinated Cd atoms were modelled as C-bound and the pseudooctahedral Cd atoms as N-bound.[37–40] In contrast to the situation for $Cd(CN)_2$ we found no crystallographic evidence of cyanide orientational disorder in $Cd(NH_3)_2[Cd(CN)_4]$.

From a geometric perspective, the topology of $Cd(NH_3)_2[Cd(CN)_4]$ is identical to that of $ZnPt(CN)_4$: formally, both are characterised by the Schläfli symbol $(4^2 \cdot 8^4)(4^2 \cdot 8^4)$. We show the two interpenetrating PtS-type nets of $Cd(NH_3)_2[Cd(CN)_4]$ in Fig. 2(c). A closely-related system containing just one such net is $Cd(NH_3)_2[Cd(CN)_4]\cdot2C_6H_6$.[41] In the non-interpenetrated system, benzene molecules occupy the pores of the single PtS net and their orientational order lowers the crystal symmetry from tetragonal to monoclinic
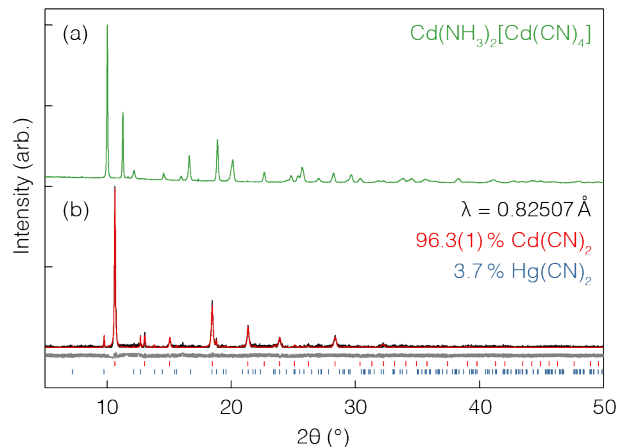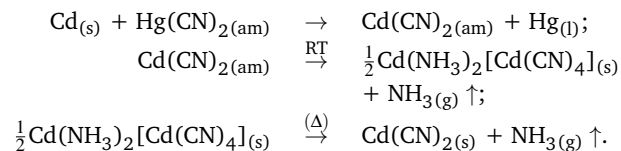
(space group $C2/c$). We note that this benzene clathrate also provides experimental precedent for the $trans$-$[Cd(NC)_4(NH_3)_2]$ coordination geometry we propose in our structural model for $Cd(NH_3)_2[Cd(CN)_4]$.

It is possible to deamminate $Cd(NH_3)_2[Cd(CN)_4]$ to give $Cd(CN)_2$ either by heating (*e.g.* at 80 °C for 24 h) or by leaving samples exposed to the atmosphere at ambient conditions for a period of 1 month. The topologies of $Cd(NH_3)_2[Cd(CN)_4]$ (doubly interpenetrating PtS) and $Cd(CN)_2$ (doubly interpenetrating diamondoid) are different, such that this deammination process is necessarily reconstructive. In Fig. 3 we show the X-ray powder diffraction patterns of the same sample before and after deammination. The post-deammination diffraction profile is well described by a Rietveld fit carried out using a two-phase mixture of $Cd(CN)_2$ (space group $Pn\bar{3}m$) and $Hg(CN)_2$ (space group $I\bar{4}2d$);[42,43] the latter component is clearly present as only a very small fraction and is discussed in more detail below. Consequently we can conclude that the primary reaction scheme observed under the conditions described here can be written as follows:

$$Cd_{(s)} + Hg(CN)_{2(am)} \rightarrow Cd(CN)_{2(am)} + Hg_{(l)};$$
$$Cd(CN)_{2(am)} \xrightarrow{RT} \tfrac{1}{2}Cd(NH_3)_2[Cd(CN)_4]_{(s)} + NH_{3(g)}\uparrow;$$
$$\tfrac{1}{2}Cd(NH_3)_2[Cd(CN)_4]_{(s)} \xrightarrow{(\Delta)} Cd(CN)_{2(s)} + NH_{3(g)}\uparrow.$$

To the best of our knowledge, this represents a new synthesis route for $Cd(CN)_2$ directly from Cd metal, and one that avoids aqueous media. We have indeed been able to replicate this synthesis on the multi-gram scale using ^{114}Cd-enriched Cd metal and our neutron scattering studies that make use of the resulting $^{114}Cd(CN)_2$ sample will form the subject of subsequent publications. We note for completeness that $Cd(CN)_2$ samples prepared in this way do not show experimental evidence of cyanide orientational order, despite the apparent presence of order within the

$Cd(NH_3)_2[Cd(CN)_4]$ intermediate. We attribute this scrambling to the reconstructive nature of the deammination process, but reserve any definitive conclusions for future NMR and/or neutron scattering studies.

3.2 Incomplete oxidation

The appearance of a small fraction of $Hg(CN)_2$ in the final deammination product of our synthesis implies that the intermediate of nominal composition $Cd(NH_3)_2[Cd(CN)_4]$ actually contains some Hg on one or both of the Cd sites, and hence that the initial oxidation of Cd by $Hg(CN)_2$ was incomplete. By varying the synthesis temperature and $Cd:Hg(CN)_2$ ratio we were able to prepare a range of (nominal) $Cd(NH_3)_2[Cd(CN)_4]$ samples that gave very different relative fractions of $Cd(CN)_2$ and $Hg(CN)_2$ in the final deammination product. We used DFT calculations to determine the most likely site for Hg substitution within the $Cd(NH_3)_2[Cd(CN)_4]$ structure and observed a very significant preference ($> 20\,kJ\,mol^{-1}$) for Hg to occupy the C-bound pseudotetrahedral site ('Cd2' in Table 1). We found this assignment to be consistent with our Rietveld analysis of the X-ray powder diffraction patterns of amminated intermediates with varying Hg content (see SI), and is consistent also with the structure proposed for the benzene clathrate $Cd(NH_3)_2[Hg(CN)_4]·2C_6H_6$.[44] Consequently we conclude that the true composition of the amminated intermediate is best described by the formula $Cd(NH_3)_2[Cd_xHg_{1-x}(CN)_4]$.

The variation in the unit cell dimensions of $Cd(NH_3)_2[Cd_xHg_{1-x}(CN)_4]$ as a function of Cd content x was determined by Rietveld analysis for four different samples and is shown in Fig. 4(a). The value of x can be determined in one of two ways: either *via* refinement of Hg occupancy on the pseudotetrahedral site in the $Cd(NH_3)_2[Cd_xHg_{1-x}(CN)_4]$ structure; or *via* refinement of the relative weight fractions of $Hg(CN)_2$ and $Cd(CN)_2$ following deammination. We find reasonable agreement between the two approaches and evidence of Vegard's law behaviour in the linear dependence of the lattice parameters on Cd/Hg content [Fig. 4(a)]. Hg-rich samples ($x \rightarrow 0$) are expanded in a and contracted in c relative to Cd-rich samples ($x \rightarrow 1$) [Fig. 4(b)]. Intriguingly, the unit cell volume actually decreases with increasing Hg content, despite the larger ionic radius of Hg^{2+} relative to Cd^{2+}:[45] we find $V = 550.847(17)\,Å^3$ for $x = 0.94$ and $545.207(17)\,Å^3$ for $x = 0.12$.

That deammination of $Cd(NH_3)_2[Cd_xHg_{1-x}(CN)_4]$ gives a physical mixture of $Cd(CN)_2$ and $Hg(CN)_2$ again indicates the reconstructive nature of this process, although in a more severe sense than the topological argument used above: there is clearly large-scale cation migration occurring even at relatively modest temperatures (*ca* 80 °C). We suggest that the difference in structure types of $Cd(CN)_2$ and $Hg(CN)_2$ is responsible for the inaccessibility of a mixed-metal $Cd_xHg_{1-x}(CN)_2$ product. This is in contrast to the experimentally-accessible family $Cd_xZn_{1-x}(CN)_2$, for which both endmembers are isostructural.[1,33,46]

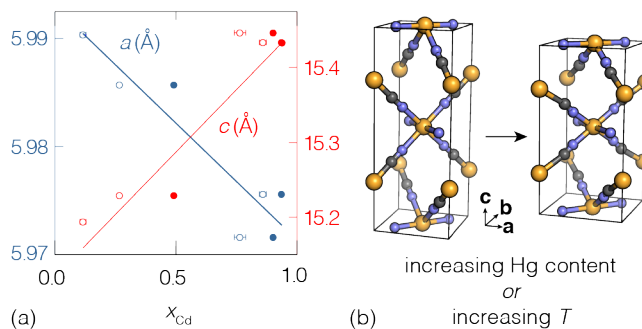**Fig. 4** (a) The variation in lattice parameters as a function of Cd content x in $Cd(NH_3)_2[Cd_xHg_{1-x}(CN)_4]$ as determined by refinement of weight percentage of $Cd(CN)_2$ and $Hg(CN)_2$ after deammination (filled circles) or refinement of Hg occupancy on the pseudotetrahedral site for $Cd(NH_3)_2[Cd_xHg_{1-x}(CN)_4]$ (open circles). The former is treated as the more reliable value because of a high correlation between Hg occupancy and atomic displacement parameters. (b) Representation of the structural effect of varying x on the unit cell dimensions.

3.3 Negative thermal expansion

Having established the ambient-temperature crystal structure of $Cd(NH_3)_2[Cd(CN)_4]$, we then sought to understand its thermal expansion behaviour. Our approach was to use variable-temperature X-ray powder diffraction measurements, from which the temperature-dependence of the lattice parameters might be extracted. The coefficients of thermal expansion are given by the normalised rate of change of each lattice parameter ℓ with temperature at constant pressure:[11]

$$\alpha_\ell = \frac{1}{\ell}\left(\frac{\partial \ell}{\partial T}\right)_p. \tag{1}$$

We used a combination of Pawley refinement in TOPAS[24] and linear strain calculations in PASCal[47] to extract values of α from our experimental X-ray powder diffraction data.

The relative variation in unit cell dimensions with temperature determined in this way is illustrated in Fig. 5. In order to extract accurate lattice parameters and to avoid beam damage, the capillary was translated by 2.5 mm for each measurement in order to expose a fresh sample to the synchrotron beam at each temperature point. We attribute the non-linearity visible from 170 K to strain induced by a small amount of residual solid mercury visible in the diffraction pattern shown in Fig. 2(a). What is clear is that the thermal expansion of $Cd(NH_3)_2[Cd(CN)_4]$ is extremely anisotropic: the compound expands along the **a** axis with increasing temperature (and hence, by the tetragonal crystal symmetry, also along **b**), but contracts along the **c** axis. The magnitude of these two responses is approximately equal: we find $\alpha_a = +27.9(5)\,MK^{-1}$ and $\alpha_c = -35.5(16)\,MK^{-1}$, see Table 2. So $Cd(NH_3)_2[Cd(CN)_4]$ exhibits uniaxial NTE and does so at a rate that is significantly larger than conventional oxide-based NTE materials (*e.g.* ZrW_2O_8,[3] $\alpha_a = -9.1\,MK^{-1}$) but smaller than the extreme values possible in other cyanide-containing frameworks (*e.g.* $Ag_3[Co(CN)_6]$,[48] $\alpha_c = -126\,MK^{-1}$). Intriguingly, the structural response of $Cd(NH_3)_2[Cd(CN)_4]$ to increasing temperature
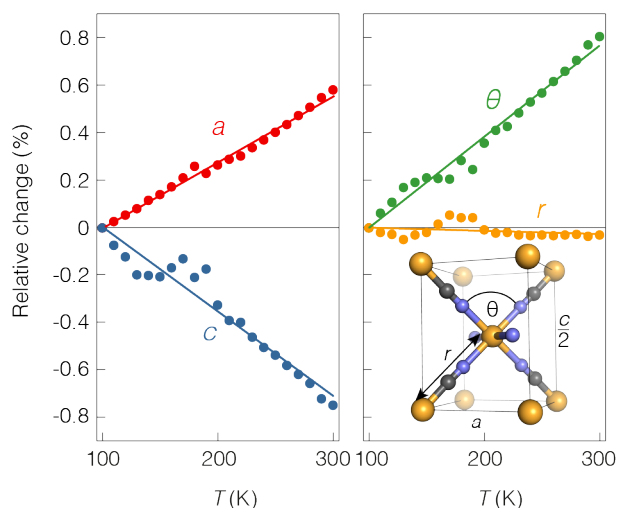
Fig. 5 The relative change in length with temperature for the a and c lattice parameters for $Cd(NH_3)_2[Cd(CN)_4]$ are shown alongside the relative changes in XBU parameters: θ and r. Their relationship to the lattice parameters is shown inset; the much greater temperature dependence of θ relative to r is indicative that it is a geometric flexing mechanism that is responsible for the large flexibility and NTE observed in this system.

mimics the effect of Cd/Hg substitution as depicted in Fig. 4(b).

For completeness we also investigated the thermal expansion behaviour of a single Hg-rich $Cd(NH_3)_2[Cd_xHg_{1-x}(CN)_4]$ sample. The specific example we consider corresponds to a Cd composition x of 0.12 on the pseudotetrahedral site; for ease we will refer to this sample hereafter using the composition $Cd(NH_3)[Hg(CN)_4]$. Our data showed a qualitatively similar thermal response to the Cd-rich endmember—again the system expands along **a** and contracts along **c** as it is heated—but the magnitude of the response is increased by 30–40% for the Hg-rich endmember (see Table 2 and SI).

To what extent is this coupled positive and negative thermal expansion response an intrinsic property of PtS-type framework materials? To answer this question we turned to the mechanical building unit (XBU) analysis of Ref. 49, whereby the framework structure is decomposed in terms of hinges and struts. The high crystal symmetry of $Cd(NH_3)_2[Cd(CN)_4]$ is such that the framework geometry is determined entirely by just two components: (i) the Cd–CN–Cd strut length r, and (ii) the CN–Cd–NC bond angle (hinge angle) θ [Fig. 5]. These two parameters are directly

related to the unit cell parameters:

$$r = \sqrt{\frac{a^2}{2} + \frac{c^2}{16}}, \qquad (2)$$

$$\theta = 2\tan^{-1}\left(\frac{2\sqrt{2}a}{c}\right). \qquad (3)$$

So, using these relationships, it is possible to recast the thermal expansion behaviour of $Cd(NH_3)_2[Cd(CN)_4]$ in terms of the variation of the XBU parameters r and θ. We show this variation in Fig. 5, where it is clear that the thermomechanical response of this system is dominated almost entirely by changes in the hinge angle θ, with the strut length r almost entirely unaffected by temperature. Such behaviour is typical of 'wine-rack' NTE systems for which changes in framework hinge angles couple positive thermal expansion (PTE) along one crystal axis to NTE along a perpendicular axis.[50] Consequently one expects uniaxial NTE in any PtS-type system in which thermal response is dominated by framework hingeing rather than bond expansion or contraction. In the case of both Cd- and Hg-containing systems—such as those we study here—the d^{10} electronic configuration presumably increases α_θ by virtue of the absence of crystal field effects.

The XBU coefficients of thermal expansion are given in Table 2 for both $Cd(NH_3)_2[Cd(CN)_4]$ and $Cd(NH_3)_2[Hg(CN)_4]$. The more extreme PTE/NTE behaviour of the Hg-rich endmember is a consequence of an increased value of α_θ. In other words, the larger Hg^{2+} cation allows a more rapid variation in framework hinge angle, which in turn translates to a more extreme PTE response along **a** and a more extreme NTE response along **c**. While we would not want to attach too much weight to the negative values of α_r for both compounds, the sign of this term is consistent with the local NTE effect of transverse vibrational modes implicated in $Zn(CN)_2$ and even $Cd(CN)_2$ itself.[1,5]

3.4 *Ab initio* calculation of elastic properties

NTE materials often exhibit a range of other anomalous mechanical and elastic responses: the geometric mechanism responsible for NTE usually also dominates the material response to strain or pressure.[51,52] In the case of $Cd(NH_3)_2[Cd(CN)_4]$, for example, its wine-rack NTE mechanism couples contraction along the **c** axis to an increase in molar volume (note $\alpha_V > 0$ in Table 2), and so the application of hydrostatic pressure—which requires volume reduction—ought to drive to an *expansion* in **c**. Such expansion-under-pressure is termed negative linear compressibility (NLC) and remains a relatively rare and attractive materials property.[53] PtS itself is thought to exhibit NLC,[54] and we conclude our study by attempting to answer the simple question of whether $Cd(NH_3)_2[Cd(CN)_4]$ also exhibits NLC and/or any other anomalous elastic responses.

Our approach is to use *ab initio* DFT methods to calculate the 0 K elastic tensor of $Cd(NH_3)_2[Cd(CN)_4]$, following the same methodology used elsewhere for a wide range of established NTE and NLC materials.[50,51] The starting point for our calculations was the lowest-temperature (100 K) experimental structure. We added hydrogens to the ammonia N atoms in the highest-

Table 2 Coefficients of thermal expansion determined using variable-temperature X-ray powder diffraction measurements and linear strain analysis.

Compound	$Cd(NH_3)_2[Cd(CN)_4]$	$Cd(NH_3)_2[Hg(CN)_4]$
α_a (MK^{-1})	27.9(5)	36.9(10)
α_c (MK^{-1})	−35.5(16)	−49.7(10)
α_V (MK^{-1})	20.3(17)	24.1(19)
α_θ (MK^{-1})	38.4(11)	51.9(13)
α_r (MK^{-1})	−1.3(7)	−2.2(16)

Table 3 Comparison between calculated and experimental structure and elastic properties of $Cd(NH_3)_2[Cd(CN)_4]$.

Lattice parameter	DFT (0 K)	Expt. (300 K)
a (Å)	6.083	5.936
c (Å)	15.63	15.548
V (Å^3)	578.3	547.85
Elastic property	Value	(Approximate) axis
K_a (TPa^{-1})	33.5	[100]
K_c (TPa^{-1})	−17.2	[001]
B (GPa)	22.8	–
E_{max} (GPa)	19.8	[111]
E_{min} (GPa)	7.35	[100]
G_{max} (GPa)	7.50	[103]
G_{min} (GPa)	2.90	[101]
v_{max}	0.790	[101]
v_{min}	−0.082	[110]

symmetry arrangement (which nevertheless breaks $P4_2/mcm$ crystal symmetry) and removed all symmetry constraints on our subsequent calculations. The resulting structure was then relaxed in $P1$ using a PBE functional implemented in the VASP code,[25–28] giving 0 K lattice parameters that are in good agreement with experimental values (differences < 2.5%, see Table 3). We expect the small discrepancy we do observe is a function of thermal effects and/or the presence of ~3% Hg in the experimental sample, in addition to the functional used.

We proceeded to calculate the full elastic tensor **C**, which in turn describes all elastic constants of interest (*e.g.* compressibilities). Because we omitted symmetry constraints, **C** contained nine independent terms; however the true tetragonal crystal symmetry was reflected in the observance of parity between terms (*e.g.* $c_{11} \simeq c_{22}$). The key elastic parameters were extracted from **C** using the ELATE code.[55] These parameters are summarised in Table 3 and form the basis for the remainder of our discussion.

The Young's modulus E is a measure of a material's resistance to uniaxial compression. The Young's moduli we calculate for $Cd(NH_3)_2[Cd(CN)_4]$ range between 7 and 20 GPa for different directions relative to the crystal axes; this variation reflects the mechanical anisotropy of the crystal structure as evident experimentally in its strongly anisotropic thermal expansion behaviour. The shear moduli G also vary by the same factor of about three. The minimum value $G_{min} = 2.90$ GPa implies that the material is likely to be elastically unstable at pressures above ~3 GPa. Shear moduli are particularly challenging to determine experimentally, as the relevant measurements (*e.g.* Brillouin or resonant ultrasound spectroscopy) typically require large single crystal samples. In the absence of a direct experimental comparison we note that the values we calculate here are similar in magnitude to those reported for other flexible framework materials.[56–58]

The elastic properties of most direct interest to the present study are the linear compressibilities, which measure the relative change in length per unit pressure change at constant temperature:

$$K_\ell = -\frac{1}{\ell}\left(\frac{\partial \ell}{\partial p}\right)_T. \qquad (4)$$

Note that a negative value of K implies a linear expansion with increasing hydrostatic pressure, and hence NLC.[53] Our data give a large and positive compressibility along the **a** crystal axis and

a less extreme but negative compressibility along the **c** crystal axis: $K_a = +33.5$ TPa^{-1} and $K_c = -17.2$ TPa^{-1}, respectively. Importantly, this NLC effect is more that two orders of magnitude stronger than that calculated for PtS itself[54]—for which $K_c = -0.08$ TPa^{-1}—yet is consistent with the behaviour observed in key NLC framework materials such as $KMn[Ag(CN)_2]_3$.[59] So $Cd(NH_3)_2[Cd(CN)_4]$ not only exhibits a relatively strong NTE effect, but our calculations indicate it is also exhibits the somewhat rarer property of NLC. As anticipated, the NTE and NLC axes coincide because the same wine-rack mechanism is activated both thermally and under hydrostatic pressure.

As a final point we note that our calculations also give the Poisson's ratios v, which measure the perpendicular strain generated by a given uniaxial stress. For most materials $v > 0$; in other words they expand laterally when compressed in any one direction.[23] $Cd(NH_3)_2[Cd(CN)_4]$ has the unusual property of a negative Poisson's ratio for compression along the $\langle 110 \rangle$ axes ($v = -0.082$). Hence the framework structure of $Cd(NH_3)_2[Cd(CN)_4]$ actually expands along the [110] axis when stretched along the [1$\bar{1}$0] axis, for example. The mechanism responsible is likely facilitated by the presence of pseudotetrahedral Cd centres.[60] It has been shown that extremes in Poisson's ratios often occur in materials with elastic anisotropy, so it is perhaps not surprising that the NLC observed here should be accompanied by a negative Poisson's ratio.[61]

4 Conclusions

Our study has achieved three key results. First, we have devised a synthetic route for $Cd(CN)_2$ which allows preparation of an isotopically enriched $^{114}Cd(CN)_2$ sample directly from Cd metal, which in turn finally opens up the possibility of studying this important NTE material using neutron scattering methods. The synthesis proceeds *via* the previously-unreported intermediate $Cd(NH_3)_2[Cd_xHg_{1-x}(CN)_4]$, where the value of x depends on the degree of oxidation of Cd metal by $Hg(CN)_2$. Our second key result is to have isolated and characterised this series of compounds, which we find to adopt the doubly-interpenetrated PtS structure type. And, third, we have shown these PtS-type cyanide frameworks exhibit a range of anomalous mechanical responses that are of interest in their own right: negative thermal expansion, negative linear compressibility, and negative Poisson's ratios. Moreover, because this behaviour arises fundamentally from geometric flexing of the PtS framework, we would expect isostructural systems—such as the $Zn[M(CN)_4]$ family[34]—to show similar responses. To the best of our knowledge, the present study is the first to have characterised thermal expansion behaviour in a PtS-type framework, and so we expect investigations of the mechanical responses of other PtS-type systems (including metal–organic frameworks) to provide obvious avenues for further research.

Conflicts of interest

There are no conflicts to declare.

Acknowledgements

References

1 A. L. Goodwin and C. J. Kepert, *Phys. Rev. B*, 2005, **71**, 140301.

2 V. E. Fairbank, A. L. Thompson, R. I. Cooper and A. L. Goodwin, *Phys. Rev. B*, 2012, **86**, 104113.

3 T. A. Mary, J. S. O. Evans, T. Vogt and A. W. Sleight, *Science*, 1996, **272**, 90–92.

4 D. J. Williams, D. E. Partin, F. J. Lincoln, J. Kouvetakis and M. O'Keeffe, *J. Solid State Chem.*, 1997, **134**, 164–169.

5 K. W. Chapman, P. J. Chupas, and C. J. Kepert, *J. Am. Chem. Soc.*, 2005, **127**, 15630–15636.

6 J. S. O. Evans, *J. Chem. Soc., Dalton Trans.*, 1999, 3317–3326.

7 G. D. Barerra, J. A. O. Bruno, T. H. K. Barron and N. L. Allan, *J. Phys.: Condens. Matter*, 2005, **17**, R217–R252.

8 C. Lind, *Materials*, 2012, **5**, 1125–1154.

9 C. P. Romao, K. J. Miller, C. A. Whiteman and M. A. White, *Negative thermal expansion (thermomiotic) materials*, Amsterdam: Elsevier, Comprehensive Inorganic Chemistry II edn, 2013.

10 J. Chen, L. Hu, J. Deng and X. Xing, *Chem. Soc. Rev.*, 2015, **44**, 3522–3567.

11 M. T. Dove and H. Fang, *Rep. Prog. Phys.*, 2016, **79**, 066503.

12 J. W. Zwanziger, *Phys. Rev. B*, 2007, **76**, 052102.

13 P. Ding, E. J. Liang, Y. Jia and Z. Y. Du, *J. Phys.: Condens. Matter*, 2008, **20**, 275224.

14 R. Mittal, M. Zbiri, H. Schober, E. Marelli, S. J. Hibble, A. M. Chippindale and S. L. Chaplot, *Phys. Rev. B*, 2011, **83**, 024301.

15 H. Fang, M. T. Dove, L. H. N. Rimmer and A. J. Misquitta, *Phys. Rev. B*, 2013, **88**, 104306.

16 I. E. Collings, A. B. Cairns, A. L. Thompson, J. E. Parker, C. C. Tang, M. G. Tucker, J. Catafesta, C. Levelut, J. Haines, V. Dmitriev, P. Pattison and A. L. Goodwin, *J. Am. Chem. Soc.*, 2013, **135**, 7610–7620.

17 B. D'Mellow, D. J. Thomas, M. J. Joyce, P. Kolkowski, N. J. Roberts and S. D. Monk, *Nucl. Instr. and Meth. Phys. Res. A*, 2007, **577**, 690–695.

18 B. F. Hoskins and R. Robson, *J. Am. Chem. Soc.*, 1990, **112**, 1546–1554.

19 F. W. Bergstrom, *J. Am. Chem. Soc.*, 1924, **46**, 1559–1568.

20 S. R. Batten and R. Robson, *Angew. Chem. Int. Ed.*, 1998, **37**, 1460–1494.

21 S. Wang, J. Bai, H. Xing, Y. Li, Y. Song, Y. Pan, M. Scheer and X. You, *Cryst. Growth Des.*, 2007, **7**, 747–754.

22 R. H. Baughman, S. Stafström, C. Cui and S. O. Dantas, *Science*, 1998, **279**, 1522–1524.

23 G. N. Greaves, A. L. Greer, R. S. Lakes and T. Rouxel, *Nat. Mater.*, 2011, **10**, 823–837.

24 A. A. Coelho, *TOPAS-Academic, version 4.1 (Computer Software)*, 2007.

25 G. Kresse and J. Hafner, *Phys. Rev. B*, 1993, **47**, 558–561.

26 G. Kresse and J. Furthmüller, *Phys. Rev. B*, 1996, **54**, 11169–11186.

27 G. Kresse and J. Furthmüller, *Comput. Mater. Sci.*, 1996, **6**, 15–50.

28 G. Kresse and D. Joubert, *Phys. Rev. B*, 1999, **59**, 1758–1775.

29 P. E. Blöchl, *Phys. Rev. B*, 1994, **50**, 17953.

30 B. Hammer, L. B. Hansen and J. K. Nørskov, *Phys. Rev. B*, 1999, **59**, 7413–7421.

31 H. T. Stokes and D. M. Hatch, *J. Appl. Cryst.*, 2005, **38**, 237–238.

32 O. Beckstein, J. E. Klepeis, G. L. W. Hart and O. Pankratov, *Phys. Rev. B*, 2001, **63**, 134112.

33 E. Shugam and H. Zhdanov, *Acta Physiochim. URSS*, 1945, **20**, 247–252.

34 A.-H. Yuan, R.-Q. Lu, H. Zhou, Y.-Y. Chen and Y.-Z. Li, *CrystEngComm*, 2010, **12**, 1382–1384.

35 A. G. Sharpe, *The Chemistry of Cyano Complexes of the Transition Metals*, Academic Press Inc. (London) Ltd., 1976.

36 K. R. Dunbar and R. A. Heintz, *Prog. Inorg. Chem.*, 1997, **45**, 283–391.

37 B. F. Abrahams, B. F. Hoskins and R. Robson, *J. Chem. Soc., Chem. Commun.*, 1990, **0**, 60–61.

38 S. Nishikiori, C. I. Ratcliffe and J. A. Ripmeester, *J. Chem. Soc., Chem. Commun.*, 1991, 735–736.

39 T. Iwamoto, S.-I. Nishikiori, T. Kitazawa and H. Yuge, *J. Chem. Soc., Dalton Trans.*, 1997, 4127–4136.

40 T. Kitazawa, S.-I. Nishikiori, R. Kuroda and T. Iwamoto, *J. Chem. Soc., Dalton Trans.*, 1994, 1029–1036.

41 H. Yuge and T. Iwamoto, *J. Incl. Phenom. Mol. Recognit. Chem.*, 1992, **14**, 217–235.

42 J. Hvoslef, *Acta Chem. Scand.*, 1958, **12**, 1568–1574.

43 R. C. Seccombe and C. H. L. Kennard, *J. Organomet. Chem.*, 1969, **18**, 243–247.

44 R. Kuroda, *Inorg. Nucl. Chem. Lett.*, 1973, **9**, 13–18.

45 R. D. Shannon, *Acta Cryst. A*, 1976, **32**, 751–767.

46 H. Zhdanov, *C. R. Acad. Sci. URSS*, 1941, **31**, 352–354.

47 M. J. Cliffe and A. L. Goodwin, *J. Appl. Crystallogr.*, 2012, **45**, 1321–1329.

48 A. L. Goodwin, M. Calleja, M. J. Conterio, M. T. Dove, J. S. O. Evans, D. A. Keen, L. Peters and M. G. Tucker, *Science*, 2008,

319, 794–797.

49 J. M. Ogborn, I. E. Collings, S. A. Moggach, A. L. Thompson and A. L. Goodwin, *Chem. Sci.*, 2012, **3**, 3011–3017.

50 A. U. Ortiz, A. Boutin, A. H. Fuchs and F.-X. Coudert, *J. Chem. Phys.*, 2013, **138**, 174703.

51 F.-X. Coudert, *Chem. Mater.*, 2015, **27**, 1905–1916.

52 L. Wang, C. Wang, H. Luo and Y. Sun, *J. Phys. Chem. C*, 2017, **121**, 333–341.

53 A. B. Cairns and A. L. Goodwin, *Phys. Chem. Chem. Phys.*, 2015, **17**, 20449–20465.

54 A. Marmier, P. S. Ntoahae, P. E. Ngoepe, D. G. Pettifor and S. C. Parker, *Phys. Rev. B*, 2010, **81**, 172102.

55 R. Gaillac, P. Pullumbi and F.-X. Coudert, *J. Phys.: Condens. Matter*, 2016, **28**, 275201.

56 D. F. Bahr, J. A. Reid, W. M. Mook, C. A. Bauer, R. Stumpf, A. J. Skulan, N. R. Moody, B. A. Simmons, M. M. Shindel and M. D. Allendorf, *Phys. Rev. B*, 2007, **76**, 184106.

57 J. C. Tan and A. K. Cheetham, *Chem. Soc. Rev.*, 2011, **40**, 1059–1080.

58 J. C. Tan, B. Civalleri, C.-C. Lin, L. Valenzano, R. Galvelis, P.-F. Chen, T. D. Bennett, C. Mellot-Draznieks, C. M. Zicovich-Wilson and A. K. Cheetham, *Phys. Rev. Lett.*, 2012, **108**, 095502.

59 A. B. Cairns, A. L. Thompson, M. G. Tucker, J. Haines and A. L. Goodwin, *J. Am. Chem. Soc.*, 2012, **134**, 4454–4456.

60 Z. Gao, X. Dong, N. Li and J. Ren, *Nano Lett.*, 2017, **17**, 772–777.

61 Z. A. D. Lethbridge, R. I. Walton, A. S. H. Marmier, C. W. Smith and K. E. Evans, *Acta Mater.*, 2010, **58**, 6444–6451.